J|A|C|S ARTICLES

Published on Web 07/06/2009

Reactions between Aromatic Hydrocarbons and Heterocycles: Covalent and Proton-Bound Dimer Cations of Benzene/Pyridine

M. Samy El-Shall,*,† Yehia M. Ibrahim,†,§ Edreese H. Alsharaeh,†,|| Michael Meot-Ner (Mautner),*,† and Simon P. Watson‡

Department of Chemistry, Virginia Commonwealth University, Richmond, Virginia 23284-2006

Received February 12, 2009; E-mail: mselshal@vcu.edu

Abstract: Despite the fact that benzene (Bz) and pyridine (Py) are probably the most common and extensively studied organic molecules, the observation of a covalent adduct in the ionized benzene/pyridine system has never been reported. This Article reports the first experimental and theoretical evidence of a covalent $(Bz\cdot Py)^{\bullet+}$ adduct that results from the reaction of $Bz^{\bullet+}$ with pyridine or $Py^{\bullet+}$ with benzene. These reactions are studied using mass-selected ion mobility, chemical reactivity, collisional dissociation, and ab initio calculations. The $(Bz\cdot Py)^{\bullet+}$ adduct does not exchange ligands with Bz to form $Bz_2^{\bullet+}$ or with Py to form $(Py)_2H^+$ despite the strong bonds in these homodimers. The thermochemistry then suggests that the $(Bz\cdot Py)^{\bullet+}$ heterodimer is bonded covalently with a bonding energy of >33 kcal/mol. Correspondingly, ab initio calculations identify covalently bonded propeller-shaped isomers of $(Bz\cdot Py)^{\bullet+}$ with bonding energies of 31−38 kcal/mol, containing a C−N bond. The mobility of the $(Bz\cdot Py)^{\bullet+}$ adduct in helium is consistent with these covalent dimers. As to noncovalent adducts, the computations identify novel distonic hydrogen-bonded complexes $(C_5H_5NH^+\cdot C_6H_5^{\bullet})$ where the charge resides on one component (PyH^+), while the radical site resides on the other component ($C_6H_5^{\bullet}$). Collisional dissociation suggests that the covalent and distonic dimers may interconvert at high energies. The most stable distonic $(C_5H_5NH^+\cdot C_6H_5^{\bullet})$ complex contains a hydrogen bond to the phenyl radical carbon site with a calculated dissociation energy of 16.6 kcal/mol. This bond is somewhat stronger than the $NH^+\cdot\pi$ hydrogen bonds of PyH^+ to the π system of the phenyl radical and of the benzene molecule. For this $NH^+\cdot\pi$ bond in the $PyH^+\cdot$Bz dimer, the measured binding energy is 13.4 kcal/mol, and ab initio calculations identify two T-shaped isomers with the NH^+ pointing to the center of the benzene ring or to the negatively charged C atoms of the ring. In contrast, the more stable proton-bound $PyH^+\cdot$Py dimer contains a linear $NH^+\cdots N$ hydrogen bond. The formation of the $(\text{benzene/pyridine})^{\bullet+}$ adduct may represent a general class of addition reactions that can form complex heterocyclic species in ionizing environments.

I. Introduction

Benzene (C_6H_6, Bz) and pyridine (C_5H_5N, Py) are prototype models of polycyclic aromatic hydrocarbons (PAHs) and aromatic nitrogen heterocycles, respectively. These compounds are common in the environment, in industry, and in biology where their cation−π interactions can affect protein structure, self-organization, molecular crystals, and molecular recognition.[1−4] Strong interactions between nitrogen containing aromatic cations and neutral π systems have been reported as significant interactions determining the protein structure.[5−8] Cations such as pyridinium and imidazolium are also common in ionic liquids.[9,10] Further, as evidenced by meteorite organics, PAHs and nitrogen heterocycles are present in space where their ion chemistry can form complex organic molecules and polymers.[11−14] Despite these various applications, little information

† Virginia Commonwealth University.

‡ Permanent address: John Curtin School of Medical Research, the Australian National University, Canberra ACT 0200, Australia.

§ Current address: Biological Sciences Division, Pacific Northwest National Laboratory, P.O. Box 999, Richland, WA 99352.

|| Current address: Department of Math and Natural Sciences, Gulf University of Sciences and Technology, P.O. Box 7207, Hawally 32093, Kuwait.

(1) Jennings, W. B.; Farrell, B. M.; Malone, J. F. *Acc. Chem. Res.* **2001**, *34*, 885–894.
(2) Hunter, C. A.; Lawson, K. R.; Perkins, J.; Urch, C. *J. Chem. Soc., Perkin Trans.* **2001**, *2*, 651–669.
(3) Hunter, C. A.; Low, C. M. R.; Rotger, C.; Vinter, J. G.; Zonta, C. *Proc. Natl. Acad. Sci. U.S.A.* **2002**, *99*, 4873–4876.
(4) Müller-Dethlefs, K.; Hobza, P. *Chem. Rev.* **2000**, *100*, 143–168.
(5) Mecozzi, S.; West, A. P., Jr.; Dougherty, D. A. *J. Am. Chem. Soc.* **1996**, *118*, 2307.
(6) Dougherty, D. A. *Science* **1996**, *271*, 163–168.
(7) Gallivan, J. P.; Dougherty, D. A. *Proc. Natl. Acad. Sci. U.S.A.* **1999**, *96*, 9459.
(8) Ma, J. C.; Dougherty, D. A. *Chem. Rev.* **1999**, *97*, 1303.
(9) Welton, T. *Chem. Rev.* **1999**, *99*, 2071–2083.
(10) Tsuzuki, S.; Tokuda, H.; Hayamizu, K.; Watanabe, M. *J. Phys. Chem. B* **2005**, *109*, 16474.
(11) Mattioda, A. L.; Hudgins, D. M.; Bauschlicher, C. W.; Rosi, M.; Allamandola, L. J. *J. Phys. Chem. A* **2003**, *107*, 1486–1498.
(12) Hudgins, D. M.; Bauschlicher, C. W.; Allamandola, L. J. *Astrophys. J.* **2005**, *632*, 316.
(13) Rhee, Y. M.; Lee, T. J.; Gudipati, M. S.; Allamandola, L. J.; Head-Gordon, M. *Proc. Natl. Acad. Sci. U.S.A.* **2007**, *104*, 5274–5278.
(14) Mattioda, A. L.; Rutter, L.; Parkhill, J.; Head-Gordon, M.; Lee, T. J.; Allamandola, L. J. *Astrophys. J.* **2008**, *680*, 1243–1255.

10.1021/ja901130d CCC: $40.75

is available on cross-reactions between ionized PAHs and nitrogen heterocycles. The nature of bond formation in cross-reactions between ionized aromatic hydrocarbons and heterocycles would be of interest, because such mixtures occur in ionizing environments. We present here such a study using $(benzene/pyridine)^{+\bullet}$ as the prototype model system.

With respect to the ion chemistry of PAHs and of nitrogen heterocycles, we previously investigated the energetics of ionization, protonation, and dimer formation,[15−19] and this thermochemistry was tabulated.[20] The kinetics of reactions of ionized PAHs with some smaller atoms and molecules were also reported,[21,22] as well as reactions of carbon clusters with pyridine.[23] Studies on related systems include the reactions of radical cations with nucleophiles in solution,[8] gas-phase studies on *N*-phenylpyridine ions,[24] and reactions of phenyl cations with *N*-heterocyclic compounds.[25] However, there seems to be no information on cross-reactions in the gas phase between neutral and ionized aromatic hydrocarbons and heterocyclic compounds.

The prototype model system for radical cation$-\pi$ interactions in the present study is the $(benzene\cdot pyridine)^{+\bullet}$ dimer radical cation. A closely related system is the benzene dimer radical cation $(Bz)_2^{+\bullet}$, whose lowest energy structure has a parallel sandwich-type structure.[19] The components of such homodimers have equal ionization energies (IEs), allowing charge transfer resonance that stabilizes the dimers.[16,17,25] Similar charge transfer resonance could stabilize the $(benzene\cdot pyridine)^{+\bullet}$ heterodimer because the IEs of Bz (9.24 eV) and Py (9.26 eV) are nearly identical.[20] However, the polarity of pyridine and the presence of the N heteroatom may allow other stable structures of the radical dimer ion. Interesting possible structures are hydrogen-bonded distonic dimers that can form if Py extracts a proton from $Bz^{+\bullet}$ to form PyH^+, which may then hydrogen bond to the remaining $C_6H_5^\bullet$ radical to form the hydrogen-bonded $C_5H_5NH^+\cdot C_6H_5^\bullet$ dimer. This would constitute a new type of distonic ion in which the charge and radical sites reside on two separate, but interacting, molecules. Covalent addition to form a single bond, multiple bonds, or fused rings may be also possible. In fact, Kenttamaa and co-workers generated charged phenyl radicals containing covalent C−N bonds with distonic structures of the type $R^+-C_6H_4^\bullet$, where R = pyridine, 2-phenyl pyridine, and 3-phenyl pyridine.[26] These charged phenyl radicals were generated by replacing a halide atom (chlorine, bromine, or iodine) in a radical cation of dihalobenzene with a nucleophile such as pyridine followed by cleaving the remaining halogen atom by collision-activated dissociation.[26−29] However, the present covalent $(Bz\cdot Py)^{+\bullet}$ adduct is different in that it retains all of the original H atoms, and there is no separate radical site, which can undergo radical reactions.[26−29] To the best of our knowledge, there are no reports in the literature for the formation of covalent adducts containing C−N bonds by gas-phase reactions of the benzene radical cation with pyridine or of the pyridine radical cation with benzene. In this Article, we shall present the first evidence by ion mobility,[30−32] collisional dissociation, and ab initio calculations of the covalent interaction in the $(Bz\cdot Py)^{+\bullet}$ dimer and discuss the structures and energetics of possible covalent and distonic isomers.

The interactions in $(Bz\cdot Py)^{+\bullet}$ involve radical ions, but closed-shell hydrogen-bonded cation$-\pi$ systems are also of interest.[8,33] For example, intramolecular pyridinium−phenyl interactions were observed by NMR shifts.[34] Very recently, high-level ab initio calculations on the pyridinium−benzene complex found a T-shaped hydrogen-bonded structure in which the N−H bond of pyridinium points toward benzene, with a binding energy of 14.77 kcal/mol.[35] We shall present the first experimental measurement of the binding energy of the closed-shell pyridinium−benzene dimer. We shall also compare structure and energetics of this dimer, where the proton resides on one pyridine moiety, with those of the proton-bound pyridine dimer (PyH^+Py), where the proton is equally shared between the two pyridine molecules.

In summary, the $(benzene\cdot pyridine)^{+\bullet}$ system provides a prototype of ionic interactions between aromatic hydrocarbons and heterocycles. We shall present new information on the stabilities and geometries of covalent and noncovalent $(benzene\cdot pyridine)^{+\bullet}$ adducts, and the hydrogen-bonded $(pyridineH^+\cdot benzene)$ dimer ion, using ion mobility, collisional dissociation, reactivity and equilibrium studies, and ab initio calculations.

II. Experimental and Computational Methods

The experiments were conducted using the VCU mass-selected ion mobility spectrometer. The details of the instrument can be found in several publications,[18,19,36] and only a brief description of the experimental procedure is given here.

The molecular ions ($pyridine^{+\bullet}$ or $benzene^{+\bullet}$) were generated by electron impact (EI) ionization of the corresponding neutral

(15) Meot-Ner (Mautner), M. *J. Phys. Chem.* **1980**, *84*, 2716–2724.
(16) El-Shall, M. S.; Kafafi, S. A.; Meot-Ner (Mautner), M.; Kertesz, M. *J. Am. Chem. Soc.* **1986**, *108*, 4386.
(17) El-Shall, M. S.; Kafafi, S. A.; Meot-Ner (Mautner), M.; Kertesz, M. *J. Am. Chem. Soc.* **1986**, *108*, 4391.
(18) Rusyniak, M.; Ibrahim, Y.; Alsharaeh, E.; Meot-Ner (Mautner), M.; El-Shall, M. S. *J. Phys. Chem. A* **2003**, *107*, 7656.
(19) Rusyniak, M. J.; Ibrahim, Y. M.; Wright, D. L.; Khanna, S. N.; El-Shall, M. S. *J. Am. Chem. Soc.* **2003**, *125*, 12001.
(20) Afeefy, H. Y.; Liebman, J. F.; Stein, S. E. Neutral Thermochemical Data; Hunter, E. P.; Lias, S. G. Proton Affinity Evaluation; Lias, S. G. Ionization Energy Evaluation; Meot-Ner (Mautner), M.; Lias, S. G. Binding Energies Between Ions and Molecules, and The Thermochemistry of Cluster Ions; Bartmess, J. E. Negative Ion Energetics Data. In *NIST Chemistry WebBook, NIST Standard Reference Database Number 69*; Linstrom, P. J., Mallard, W. G., Eds.; National Institute of Standards and Technology: Gaithersburg, MD, June 2005; p 20899 (http://webbook.nist.gov).
(21) Le Page, V.; Keheyan, Y.; Snow, T. P.; Bierbaum, V. M. *J. Am. Chem. Soc.* **1999**, *121*, 9435–9446.
(22) Betts, N. B.; Stepanovic, M.; Snow, T. P.; Bierbaum, V. M. *Astrophys. J.* **2006**, *651*, L129–L131.
(23) Pozniak, B. P.; Dunbar, R. C. *J. Am. Chem. Soc.* **1997**, *119*, 7343.
(24) Parker, V. D. *Acc. Chem. Res.* **1984**, *17*, 243.
(25) Meot-Ner (Mautner), M.; Hamlet, P.; Hunter, E. P.; Field, F. H. *J. Am. Chem. Soc.* **1978**, *100*, 5466.
(26) Thoen, K. K.; Smith, R. L.; Nousiainen, J.; Nelson, E. D.; Kenttämaa, H. I. *J. Am. Chem. Soc.* **1996**, *118*, 8669.
(27) Smith, R. L.; Kenttämaa, H. I. *J. Am. Chem. Soc.* **1995**, *117*, 1393.
(28) Tichy, S. E.; Thoen, K. K.; Price, J. M.; Ferra, J. J.; Petucci, C. J.; Kenttämaa, H. I. *J. Org. Chem.* **2001**, *66*, 2726.
(29) Tichy, S. E.; Nelson, E. D.; Amegayibor, F. S.; Kenttämaa, H. I. *J. Am. Chem. Soc.* **2004**, *126*, 12957.
(30) von Helden, G.; Wyttenbach, T.; Bowers, M. T. *Science* **1995**, *267*, 1483–1485.
(31) Summers, M. A.; Kemper, P. R.; Bushnell, J. E.; Robinson, M. R.; Bazan, G. C.; Bowers, M. T.; Buratto, S. K. *J. Am. Chem. Soc.* **2003**, *125*, 5199.
(32) Shvartsburg, A. A.; Hudgins, R. R.; Dugourd, P.; Jarrold, M. F. *J. Phys. Chem.* **1997**, *101*, 1684.
(33) Meot-Ner (Mautner), M. *Chem. Rev.* **2005**, *105*, 213.
(34) Acharya, P.; Plashkevych, O.; Morita, C.; Yamada, S.; Chattopadhyaya, J. *J. Org. Chem.* **2003**, *68*, 1529–1538.
(35) Tsuzuki, S.; Mikami, M.; Yamada, S. *J. Am. Chem. Soc.* **2007**, *129*, 8656.
(36) El-Shall, M. S. *Acc. Chem. Res.* **2008**, *41*, 783–792.

Scheme 1

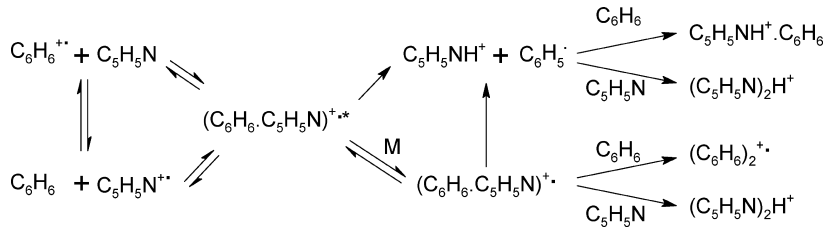

molecular clusters formed by expanding 6.9 bar of ultra pure helium seeded with 0.5% of pyridine (Py) or benzene (Bz) vapor through a pulsed nozzle into a vacuum chamber (10^{-7} mbar). Deuterated benzene C_6D_6 (*m*/*z* 84) was used in several experiments to duplicate the results obtained with C_6H_6 (*m*/*z* 78) and to provide better mass separation with pyridine (*m*/*z* 79). To form the protonated or the deuterated species, the pyridine vapor was coexpanded with methanol or CD_3OD, and the mixed neutral clusters were ionized by EI. In all cases, the molecular ions of interest were mass selected in a quadrupole mass filter and injected (in 5−15 μs pulses) into a drift cell (the inner diameter and length of the cell are 8.1 and 8.9 cm, respectively) filled with pure helium, or Bz or Py vapor in He. Flow controllers (MKS # 1479A) were used to maintain a constant pressure inside the drift cell. Mass spectra were obtained of ions exiting from the mobility cell. Arrival time distributions (ATDs) of the various ions were measured by monitoring the signals corresponding to each ion as a function of time after injection into the cell. Varying the cell voltage changes the residence times of the ions, usually between 200 and 1500 μs after injection. Such time-resolved studies determine if products are formed due to high-energy injection or due to reactions in the cell, and allow identifying primary and secondary reaction products and measuring rate coefficients.

Pseudo first-order rate constants were calculated using $\ln I/\sum I = -kt$, where I is the integrated intensity of the reactant ion mobility peak and $\sum I$ is sum of the intensities of the reactant and all product ion peaks including secondary products, and t is the mean drift time, taken as the center of the arrival time distribution of the reactant ion. In time-resolved experiments, we obtained k from plots of $\ln I/\sum I$ versus t, where we varied the reaction time by changing the drift voltage, and obtained pseudo-first-order rate coefficients k_1 from the slopes of the plots.

Second-order rate constants k_2 were obtained from $k_2 = k_1/[N]$, where N is the number density (molecules cm^{-3}) of the neutral reactant Bz or Py, calculated from the equilibrium pressure of the reactant over a reservoir in which its vapor is mixed with the He carrier gas at a known temperature. At very low concentrations of Bz or Py, the number density was determined by measuring k_1 of a reaction with known rate constant k_2 and calculating $[N]$ from the above equation. We used the reaction of $O_2^{\bullet+}$ with C_6H_6, which proceeds at a collision rate of 1.6×10^{-9} cm^3 s^{-1} and with C_5H_5N that proceeds at a collision rate of 2.6×10^{-9} cm^3 s^{-1} to calibrate the system.[37,38]

We also studied products of collisional dissociation and higher-energy reactions upon the injection of ions into the cell. The mass-selected ions undergo a large number of collisions with helium atoms or reactant neutral molecules at the entrance to the drift cell because the helium buffer gas and the neutral molecules flow out of the drift cell through the entrance and exit pinholes of the cell. The significance of the direct collisions of the high-energy ions with Bz or Py near the entry pinhole increases with increasing mole fraction of these reactants in He. The energy of the collisions can be varied by varying the injection energy, from 10 to 90 eV depending on the mass of the injected ion.

Equilibrium constants for the association of PyH^+ with Bz were calculated from $K = [I(PyH^{\bullet+}Bz)/I(PyH^+)P(Bz)]$, where I is integrated peak intensity and $P(Bz)$ is the partial pressure of Bz (atm) in the drift cell. The establishment of the equilibrium was verified by two criteria: (1) no change in the ratio of the product to reactants as the reaction time was changed by varying the drift voltage; and (2) equal arrive time distributions (ATDs) for the reactants and products, indicating equal residence times.

Ion mobility measurements were done by injecting an ion pulse of 10−50 μs into the drift cell. ATDs with 2 μs resolution were determined at different P/V values, where P is the He pressure in Torr and V is the drift voltage in volts, by varying V while keeping P fixed. The plot of the mean arrival time versus P/V gives a straight line, and the reduced mobility is calculated from the slope of the equation $t = [(z^2 \times 273.15)/(T \times 760 \times K_0)](P/V) + t_0$. Here, t is the mean arrival time, z is the drift cell length, T (K) is the cell temperature, K_0 is the reduced mobility, and t_0 is the time that the ions spend outside the cell.[39,40] Structural characterization was performed by measuring the reduced mobilities of ions and comparing these with the mobilities of ions with various structures calculated using the MOBCAL program.[41]

The ab initio calculations examined several $(C_6H_6 \cdot C_5H_5N)^{\bullet+}$ adducts, optimized at UB3LYP/6-311G(d,p) level. The calculations were performed using the Gaussian 98 program package.[42] The optimized structures were confirmed to be minima by vibrational frequency analysis.

III. Results and Discussion

1. Reactions and Energetics. The actual and potential ionic reactions in the $Bz^{+\bullet}$ + Py and $Py^{+\bullet}$ + Bz systems are shown in Scheme 1.

Ion−molecule reactions proceed through an activated complex. The reaction between $Bz^{\bullet+}$ and Py may lead to proton transfer or charge transfer (because the IEs of Bz (9.24 eV) and Py (9.26 eV) are nearly identical). In the forward direction, the activated complex $(Bz \cdot Py)^{+\bullet}$* may dissociate to form $Py^{+\bullet}$ + Bz, which constitutes charge transfer from $Bz^{\bullet+}$ to Py, or to form $PyH^+ + C_6H_5^{\bullet}$, which constitutes proton transfer from $Bz^{\bullet+}$ to Py. Alternatively, the activated complex may be stabilized collisionally or radiatively to form the stabilized $(Bz \cdot Py)^{\bullet+}$ adduct. The adduct may be stable, or it may dissociate thermally back to the reactants or to yield the proton transfer products. The primary products may react further in the association or ligand exchange reactions shown in Scheme 1. Table 1 shows the thermochemistry of the observed species.

2. Observed Reactions and Products. Figure 1 displays typical mass spectra obtained following the injection of the

(37) Spanel, P.; Smith, D. *Int. J. Mass Spectrom. Ion Processes* **1998**, *76*, 203.
(38) Arnold, S. T.; Williams, S.; Dotan, I.; Midey, A. J.; Morris, R. A.; Viggiano, A. A. *J. Phys. Chem. A* **1999**, *103*, 8421.
(39) Mason, E. A.; McDaniel, E. W. *Transport Properties of Ions in Gases*; Wiley: New York, 1988.
(40) Ibrahim, Y.; Alshraeh, E.; Dias, K.; Meot-Ner (Mautner), M.; El-Shall, M. S. *J. Am. Chem. Soc.* **2004**, *126*, 12766.
(41) Mesleh, M. F.; Hunter, J. M.; Shvatsburg, A. A.; Schatz, G. C.; Jarrold, M. F. *J. Phys. Chem.* **1996**, *100*, 16082.
(42) Frisch, M. J.; *Gaussian 98*, revision A.9; Gaussian, Inc.: Pittsburgh, PA, 1998.

Table 1. Thermochemical Properties of Ions and Neutrals Related to the (Benzene/Pyridine)$^{\bullet+}$ Reaction System[a]

	ΔH^o_f (B)	IE (eV)	PA	ΔH^o_f ($B^{\bullet+}$)[b]	ΔH^o_f (BH^+)[c]	ΔH^o_D[d]	ΔS^o_D[d]	ΔH^o_f ($B_2^{\bullet+}$)[e]
H	52.1	13.60		365.7				
$C_6H_5^\bullet$	81		213.8					
C_6H_6	19.8	9.24		232.9				
$(C_6H_6)_2^{\bullet+}$						17.6[f]	27.1[f]	235.1
$C_5H_4N^\bullet$	86.5[g]		204.5					
C_5H_5N	33.5	9.26	222.0	247.0	177.2			
$(C_5H_5N)_2H^+$						25.2[h]	29.7[h]	185.5
$C_5H_5NH^{\bullet+}\cdot C_6H_6$						13.4[i]	25.1[i]	

[a] Units: ΔH^o kcal/mol, ΔS^o cal/(mol K), IE in eV, based on data in ref 20. [b] ΔH^o_f ($B^{\bullet+}$) = ΔH^o_f (B) + IE (B) (using stationary electron convention). [c] ΔH^o_f (BH^+) = ΔH^o_f (B) + ΔH^o_f (H^+) − PA (B). [d] Dissociation enthalpy (kcal/mol) and entropy (cal/(mol K)) of the complex in column 1. [e] ΔH^o_f ($B_2^{\bullet+}$) = ΔH^o_f ($B^{\bullet+}$) + ΔH^o_f (B) − ΔH^o_D and similarly for the protonated dimer. [f] Thermochemistry from ref 18. [g] ΔH^o_f ($C_5H_4N^\bullet$) = ΔH^o_f ($C_5H_4N^-$) + EA (C_5H_4N) based on data in ref 20. [h] Thermochemistry from ref 20. [i] Results from this study. Estimated uncertainty, ΔH^o_D, ±0.6 kcal mol^{-1}, and ΔS^o_D, ±2 cal mol^{-1} K^{-1}.

mass-selected $C_6D_6^{\bullet+}$ or $C_5H_5N^{\bullet+}$ ions into the drift cell containing C_5H_5N/He or C_6D_6/He vapor mixtures, respectively. At lower concentrations of pyridine (Figure 1a), the major reaction product with $C_6D_6^{\bullet+}$ is the $(C_6D_6\cdot C_5H_5N)^{\bullet+}$ adduct and minor products resulting from the exothermic proton transfer (PT) from $C_6D_6^{\bullet+}$ to C_5H_5N followed by association with neutral C_5H_5N to form the protonated pyridine dimer $(C_5H_5N)_2D^+$. Also, the charge transfer channel from $C_6D_6^{\bullet+}$ to C_5H_5N is observed. This channel is followed by a proton transfer from $C_5H_5N^+$ to C_5H_5N and subsequent association to form $(C_5H_5N)_2H^+$.

At higher pyridine concentrations (Figure 1b), the $(C_5H_5N)_2H^+$ and the $(C_6D_6\cdot C_5H_5N)^{\bullet+}$ adducts are the only products. Similarly, the $(C_6D_6\cdot C_5H_5N)^{\bullet+}$ adduct is the major product resulting from the reaction of $C_5H_5N^{\bullet+}$ with C_6D_6 at lower concentrations of C_6D_6 as shown in Figure 1c. Minor channels corresponding to the exothermic charge transfer (CT) from $C_5H_5N^{\bullet+}$ to C_6D_6 and hydrogen (deuteron) transfer (HT) from C_6D_6 to $C_5H_5N^{\bullet+}$ are also observed. However, these channels become more significant along with the formation of benzene dimer cation $(C_6D_6)_2^{\bullet+}$ at higher concentrations of benzene as shown in Figure 1d. Table 2 summarizes the observed primary and secondary reactions along with other possible reactions in the $C_6D_6^{\bullet+}$ + C_5H_5N or the $C_5H_5N^{\bullet+}$ + C_6D_6 systems, and the specific reactions are discussed below.

2.a. Reactions of Benzene$^{\bullet+}$ with Pyridine. Figure 2 shows the ATDs of the ions observed after $C_6D_6^{\bullet+}$ was injected into Py/He, and Table 2 summarizes the primary reactions 1−3 and product distributions in this system. The measured rate coefficient for the overall reaction $Bz^{\bullet+}$ + Py → products is 1.8 × 10^{-9} cm^3 s^{-1}, near the collision rate.

The reactant ions $C_6D_6^{\bullet+}$ and the proton transfer product ions $C_5H_5ND^+$ have similar geometries, leading to similar mobilities and ATDs. In contrast, the adduct ion $(C_5H_5N\cdot C_6D_6)^{\bullet+}$ has a larger cross-section, lower mobility, and longer ATD. Some of these adducts form near the exit pinhole from reactant $C_6D_6^{\bullet+}$ ions that moved through the cell because of its greater mobility, contributing to the short-time edge of the adduct ion peak. At the other extreme, some adducts form already near the entrance and move slowly through the whole length of the cell, contributing to the long-time edge of the adduct ATD peak. Other adduct ions that form in between, and diffusion, broaden the ATD of the $(Bz\cdot Py)^{\bullet+}$ adduct ions. The adduct ion peak does not overlap with the $Bz^{\bullet+}$peak, which shows the absence of association−dissociation equilibrium. This shows that the adduct is formed irreversibly, and does not dissociate thermally under the experimental conditions.

2.b. Reactions of Pyridine$^{\bullet+}$ with Benzene. The arrival time distributions of the reactants and the products when $Py^{\bullet+}$ was injected into C_6D_6/He at a low partial pressure of C_6D_6 in the cell are given in the Supporting Information (SI-1). Table 2 summarizes the primary reactions 4−6 and their rates in this system.

Similar to Figure 2, the main product is again the $(Bz\cdot Py)^{\bullet+}$ adduct with a broad tailed ATD (SI-1). The irreversible addition of $C_5H_5N^{\bullet+}$ onto C_6D_6 at the entrance and across the drift cell is clearly demonstrated by the shape and broadening of the ATD of the $(Bz\cdot Py)^{\bullet+}$ ion. The observed product PyD^+ (*m*/*z* 81) confirms D atom transfer from C_6D_6, and the charge transfer product ($C_6D_6^{\bullet+}$) was also observed (SI-1). The measured rate coefficient for the overall reaction $Py^{\bullet+}$ + Bz → products is 1.6 × 10^{-9} cm^3 s^{-1}, near the collision rate. When the partial pressure of benzene is increased, the $Bz^{\bullet+}$ charge transfer product reacts further rapidly to yield the $(Bz_2)^{\bullet+}$ radical dimer ion in equilibrium with the monomer ion (reaction 7, Table 2).

A time-resolved study is illustrated in Figure 3. The abundance of the reactant $Py^{\bullet+}$ ion decreases with time, and the abundance of the main product ion $(Bz\cdot Py)^{\bullet+}$ increases. The smaller $C_6D_6^{\bullet+}$ and $C_5H_5ND^+$ products are approximately constant in abundance, suggesting that they may be formed at early times, possibly by high-energy reactions upon injection, and do not undergo further thermal reactions.

It is clear that the main channel in the $C_6D_6^{\bullet+}$ + C_5H_5N or the $C_5H_5N^{\bullet+}$ + C_6D_6 reactions is the association that proceeds near the collision rate in 1.5 Torr He buffer gas to form the $(C_5H_5N\cdot C_6D_6)^{\bullet+}$ adduct. This shows that under these conditions the excited complex $(Bz\cdot Py)^{\bullet+}$* in Scheme 1 does not dissociate back to reactants. PT constitutes <10% and CT <2% in the $Bz^{\bullet+}$/Py system. HT and CT constitute <20% and <5%, respectively, in the $Py^{\bullet+}$/Bz system.

2.c. Collisional Dissociation of the $(Bz\cdot Py)^{\bullet+}$ Adduct. We observed that the dissociation of the collisionally excited $(Bz\cdot Py)^{\bullet+}$* contributes to proton transfer and charge transfer products. We observed these products by generating the $(Bz\cdot Py)^{\bullet+}$ adduct by EI ionization of the neutral (benzene) (pyridine) clusters formed by supersonic jet expansion. The adducts were then injected into He at injection energies of 15−40 eV (lab coordinates), and the resulting mass spectrum identified the major dissociation product as PyH^+ with very minor products from $Bz^{\bullet+}$ and $Py^{\bullet+}$ (Supporting Information, SI-2).

Figure 4 shows the effect of the injection energy on the dissociation products of the $(Bz\cdot Py)^{\bullet+}$ adduct. Reaction 4 (Table 2) shows that the dissociation of the $(Bz\cdot Py)^{\bullet+}$ adduct to $Bz^{\bullet+}$ + Py is higher in energy by 7.8 kcal mol^{-1} than dissociation to PyH^+ + $C_6H_5^\bullet$ products (Reaction 2). Correspondingly, the ratio of the higher energy to lower energy products $Bz^{+\bullet}$/PyH^+

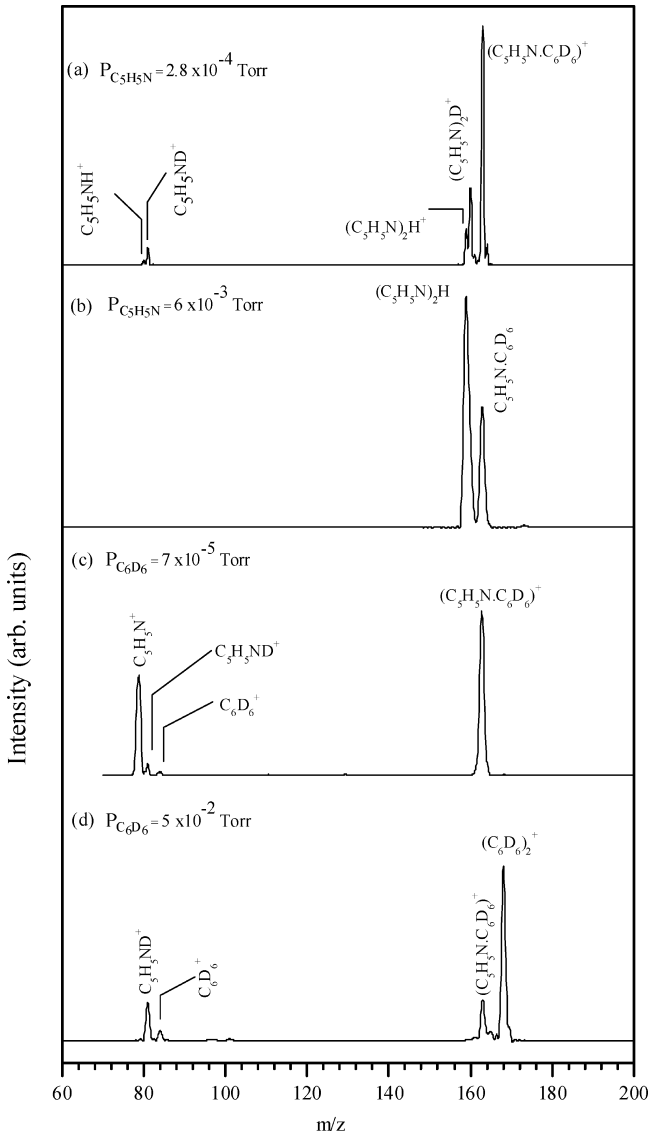

Figure 1. (a) Mass spectrum of $C_6D_6^{+\bullet}$ injected (injection energy = 15 eV lab.) into C_5H_5N/He at a partial pressure of 2.8×10^{-4} Torr in 1.4 Torr He at $T = 303$ K. (b) Mass spectrum of $C_6D_6^{+\bullet}$ injected (injection energy = 14 eV lab.) into C_5H_5N/He at a partial pressure of $C_5H_5N = 6.1 \times 10^{-3}$ Torr in 1.4 Torr He at a field of 1.81 V Torr^{-1} cm^{-1} and $T = 303$ K. (c) Mass spectrum of $C_5H_5N^{+\bullet}$ injected (injection energy = 15 eV lab.) into C_6D_6/He at low partial pressure of $P(C_6D_6) = 7.0 \times 10^{-5}$ Torr in 1.7 Torr He at a field of 1.33 V Torr^{-1} cm^{-1} and $T = 303$ K. (d) Mass spectrum of $C_5H_5N^{+\bullet}$ injected (injection energy = 11 eV lab.) into C_6D_6/He at a partial pressure of $C_6D_6 = 5.0 \times 10^{-2}$ Torr in 2.0 Torr He at a field of 0.86 V Torr^{-1} cm^{-1} and $T = 342$ K.

increases with increasing injection energy from 0.5 at 20 eV to 0.7 at 30 eV and 0.9 at 40 eV according to the plots in Figure 4.

The dissociation products are consistent with a noncovalent $(Bz\cdot Py)^{+\bullet}$ adduct or an adduct bonded by a single C−N covalent bond, in that no fragments contain more carbon atoms than the monomer reactants were observed. This suggests that the adduct does not contain covalently fused rings.

Figure 4 and the mass spectrum given in the Supporting Information (SI-2) suggest that at the lowest collision energy for dissociation, at about 15 eV (lab), the main product is $C_5H_5ND^+ + C_6D_5^\bullet$, corresponding to a complex where a deuteron was transferred to Py. This may suggest that the adduct could have a distonic structure such as $C_5H_5ND^+\cdots C_6D_5^\bullet$ or a covalent structure such as $(C_5H_5DN-C_6D_5)^{+\bullet}$. Both structures involve a deuteron transfer from C_6D_6 to the pyridine moiety C_5H_5N. These and other possible structures will be discussed below.

2.d. Bond Strength of $(Bz\cdot Py)^{+\bullet}$ Estimated from Ligand Exchange Energetics. The dissociation of noncovalently bonded clusters usually does not involve reverse activation energies, as established by metastable and CID dissociation of dimers in the Kinetic Method.[43] In the absence of such barriers, exothermic ligand exchange reactions can also occur rapidly.[43] In the present system, we tested ligand exchange reactions of the $(Bz\cdot Py)^{+\bullet}$ adduct with further Bz or Py molecules. In the first test, the adduct $(C_6D_6\cdot C_5H_5N)^{+\bullet}$ was injected into C_6D_6/He at $P(C_6D_6) = 4.0 \times 10^{-2}$ Torr at 303 K, and the resulting mass spectrum, shown in Figure 5a, indicates no exchange reaction occurred to form $(C_6D_6)_2^{+\bullet}$. The minor $(C_6D_6)_2^{+\bullet}$ peak was formed at early time and was approximately constant, suggesting that it was formed by the reaction of $C_6D_6^{+\bullet}$ generated by higher energy collisions upon injection. The measured rate coefficient of reaction 11 (Table 2) was $k_{11} < 7 \times 10^{-13}$ cm^3 s^{-1}.

The non-occurrence of ligand exchange suggests that reaction 11 (Table 2) is endothermic, that is, that $\Delta H^o_{11} > 0$. Considering the reactions in Table 2, then $\Delta H^o_{11} = \Delta H^o_7 + \Delta H^o_{14} = \Delta H^o_{14} - 17.6$ kcal/mol > 0, giving $\Delta H^o_{14} > 17.6$ kcal mol^{-1} as the lower limit for the dissociation energy of the adduct.

In further experiments, we injected the adduct $(C_6D_6\cdot C_5H_5N)^{+\bullet}$ into Py/He at a Py partial pressure of 8.0×10^{-3} Torr at 303 K, and the ion drift time was varied from 1.2 to 1.9 ms. Because the ion $(C_5H_5N)_2D^+$ at m/z 160 was not observed as shown in Figure 5b, we conclude that the ligand exchange reaction (reaction 12, Table 2) did not occur. The observed small peak corresponding to $(C_5H_5N)_2H^+$ at m/z 159 results from the dissociation of the $(C_6D_6\cdot C_5H_5N)^{+\bullet}$ into $C_6D_5^\bullet + C_5H_5ND^+$ (reaction 13, Table 2) followed by H/D exchange and association with C_5H_5N to form $(C_5H_5N)_2H^+$ (reaction 9, Table 2). Because of the higher pressure of pyridine (C_5H_5N) in the drift cell (8.0×10^{-3} Torr), the H/D exchange is very efficient, and no $C_5H_5ND^+$ is observed.

The nonreactivity of $(Bz\cdot Py)^{+\bullet}$ suggests that reaction 12 is endothermic with $\Delta H^o_{12} > 0$ kcal mol^{-1}. Considering that $\Delta H^o_{12} = \Delta H^o_2 + \Delta H^o_9 + \Delta H^o_{14}$ (see Table 2), this yields $\Delta H^o_{14} > 33.4$ kcal mol^{-1} as the lower limit for the bond dissociation energy of $(Bz\cdot Py)^{+\bullet}$ to $Bz^{+\bullet} + Py$. This bond energy gives the enthalpy of the adduct $\Delta H^o_f\,(Bz\cdot Py)^{+\bullet} < 233$ kcal mol^{-1}. From this value, we can also calculate the dissociation energy of the $(Bz\cdot Py)^{\bullet\,+}$ adduct to $C_5H_5NH^+ + C_6H_5^\bullet$ as $\Delta H^o_{13} > 25.2$ kcal/mol (reaction 13, Table 2).

Finally, the theoretical calculations below show distonic complexes $(C_5H_5NH^+\cdot C_6H_5^\bullet)$ with dissociation energies <17 kcal mol^{-1} to the $C_5H_5NH^+ + C_6H_5^\bullet$ components. This is smaller than the binding energy of 25.2 kcal mol^{-1} of the $(C_5H_5N)_2H^+$ dimer. Therefore, the distonic complexes should readily exchange ligands in Py/He gas to form the protonated pyridine dimer, but this was not observed.

In summary, the absence of ligand-exchange reactions of the $(Bz\cdot Py)^{+\bullet}$ adduct with Bz or Py (Reactions 11 and 12, respectively) suggests that the binding energy with respect to the separated $Bz^{+\bullet} + Py$ reactants is >17.6 or >33.4 kcal mol^{-1}, respectively, the latter suggesting a covalent adduct.

2.e. Binding Energy of the Pyridinium−Benzene ($PyH^+\cdot Bz$) Complex. For comparison with the radical cation $(Bz\cdot Py)^{+\bullet}$

(43) Cooks, R. G.; Koskinen, J. T.; Thomas, P. D. *J. Mass Spectrom.* **1999**, *34*, 85.

Table 2. Rate Coefficients, Product Distributions, and Thermochemistry in the (Benzene/Pyridine)$^{+\bullet}$ System

	reactants	products	k (10^{-9} cm^3/s)	branching ratio	ΔH^{o}[a]	reaction type[b]
		Primary Reactions				
1	$C_6D_6^{\bullet+} + C_5H_5N$	$C_5H_5N^{\bullet+} + C_6D_6$	1.8 ± 0.6[c]	<0.02	+0.4	CT
2		$C_5H_5ND^+ + C_6D_5^{\bullet}$		<0.1	−8.2	PT
3		$(C_6D_6{\bullet}C_5H_5N)^{\bullet+}$		>0.9	<−33.4[d]	assoc
4	$C_5H_5N^{\bullet+} + C_6D_6$	$C_6D_6^{\bullet+} + C_5H_5N$	1.6 ± 0.6[c]	<0.05	−0.4	CT
5		$C_5H_5ND^+ + C_6D_5^{\bullet}$		<0.2	−8.6	HT
6		$(C_6D_6{\bullet}C_5H_5N)^{\bullet+}$		>0.75	<−33.8[d]	assoc
		Secondary Reactions				
7	$C_6D_6^{\bullet+} + C_6D_6$	$(C_6D_6)_2^{\bullet+}$			−17.6	assoc
8	$C_5H_5N^{\bullet+} + C_5H_5N$	$C_5H_5NH^+ + C_5H_4N^{\bullet}$			−16.8	PT
9	$C_5H_5NH^+ + C_5H_5N$	$(C_5H_5N)_2H^+$			−25.2	assoc
10	$C_5H_5NH^+ + C_6D_6$	$(C_5H_5NH^+{\bullet}C_6D_6)$			−13.4[e]	assoc
11	$(C_6D_6{\bullet}C_5H_5N)^{\bullet+} + C_6D_6$	$(C_6D_6)_2^{\bullet+} + C_5H_5N$	<0.001		>0[f]	LS
12	$(C_6D_6{\bullet}C_5H_5N)^{\bullet+} + C_5H_5N$	$(C_5H_5N)_2D^+ + C_6D_5^{\bullet}$	<0.001		>0[f]	HT + LS
13	$(C_6D_6{\bullet}C_5H_5N)^{\bullet+}$	$C_6D_5^{\bullet} + C_5H_5ND^+$			>25.2[d,g]	HT + dissoc
14	$(C_6D_6{\bullet}C_5H_5N)^{\bullet+}$	$C_6D_6^{\bullet+} + C_5H_5N$			>33.4[d,g]	dissoc
15	$(C_6D_6{\bullet}C_5H_5N)^{\bullet+}{\bullet}C_5H_5N$	$(C_6D_6{\bullet}C_5H_5N)^{\bullet+} + C_5H_5N$			12.5[h]	dissoc

[a] Units are in kcal/mol, calculated from data in ref 20. [b] CT, charge transfer; HT, hydrogen atom transfer; PT, proton transfer; LS, ligand switching. Some of the data were obtained from reactions using C_6D_6. [c] Rate constants for the overall forward reaction into all of the channels. Error estimates from the measured range of results in replicate measurements. [d] Estimated from the absence of ligand switching; see text. [e] Present work. $\Delta H^0_{10} = -13.4 \pm 0.6$ kcal mol^{-1}, $\Delta S^o_{10} = -25.1 \pm 2$ cal/(mol K). Error estimates from standard deviation of slope and intercept of van't Hoff plot. [f] These ligand transfer reactions are not observed and assumed to be endothermic. [g] Based on the assumed endothermicity of reaction 12. [h] From measured ΔG^o_D (300) = 5.0 kcal mol^{-1} (this work) and $\Delta S^o_D = 25$ cal mol^{-1} K^{-1}, estimated. The reversibility of the reaction and the binding energy suggest a hydrogen-bonded complex.

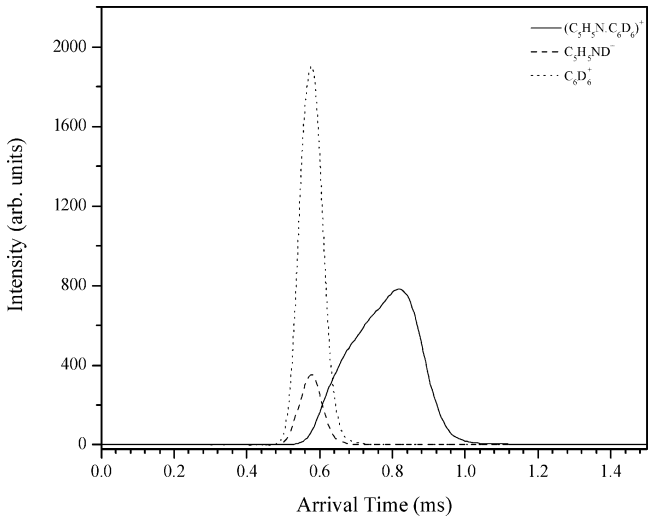

Figure 2. Arrival time distributions and intensities of ions observed after injection of $C_6D_6^{\bullet+}$ (injection energy = 15 eV lab.) into C_5H_5N/He at low partial pressure of C_5H_5N at $P(C_5H_5N) = 2.9 \times 10^{-6}$ Torr in 1.5 Torr He at a field of 1.80 V Torr^{-1} cm^{-1} and $T = 304$ K.

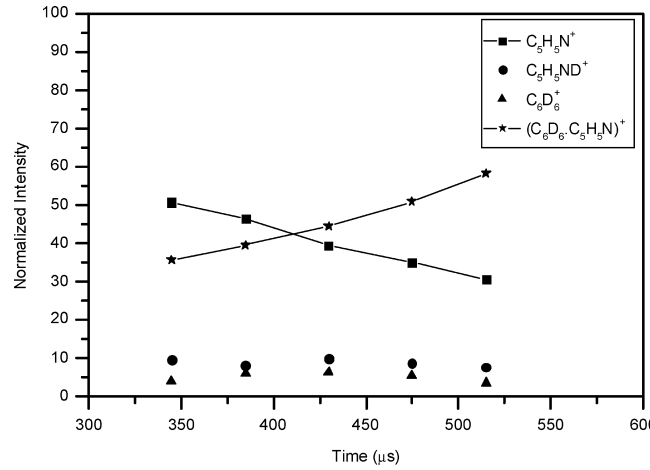

Figure 3. Time-resolved study in $C_5H_5N^{\bullet+}$ injected into C_6D_6/He in the mobility cell with 18 eV kinetic energy (laboratory) at 371 K, $P(C_6D_6) = 2.0 \times 10^{-4}$ Torr; P(He) = 1.4 Torr. The time was varied by varying the field from 1.6 to 2.6 V Torr^{-1} cm^{-1}. Ion intensities at each time represent the normalized intensity $I/\sum I$, where I is the area of the ATD peak and $\sum I$ is the sum of areas of all peaks. The time scale represents the arrival time of the maximum of the ATD peak of the $C_5H_5N^{\bullet+}$ reactant ion at each cell voltage, including time spent outside the cell.

adduct, we investigated the association of the closed-shell protonated pyridine (pyridinium ion, PyH^+) with benzene. The PyD^+ was mass-selected from CD_3OD-pyridine cluster ions formed by EI ionization of the neutral clusters. The mass-selected PyD^+ was injected into the drift cell containing pure benzene vapor, and the establishment of equilibrium was verified by the identical ATDs of the PyD^+ and $PyD^+{\bullet}Bz$ ions shown in Figure 6a. The equilibrium constant for the association of PyD^+ with benzene (reaction 10, Table 2) measured at different temperatures yields the van't Hoff plot shown in Figure 6b.

From the slope and intercept of the van't Hoff plot shown in Figure 6b, ΔH^o_D and ΔS^o_D for the formation of the $(PyD^+{\bullet}Bz)$ complex were found to be 13.4 kcal mol^{-1} and 25.1 cal mol^{-1} K^{-1}, respectively. These values are consistent with the usual range for the $NH^+{\bullet}\pi$ ionic hydrogen-bonded complexes.[33,44] However, the binding energy in this system is significantly smaller than that in the $(C_5H_5NH^+{\bullet}NC_5H_5)$ proton-bound pyridine dimer where $\Delta H^o_D = 25.2$ kcal mol^{-1} due to stronger interactions between the proton and the lone pair of the pyridine nitrogen.[33] As expected, the binding energies of the closed-shell hydrogen-bonded $(PyD^+{\bullet}Bz)$ and $(PyH^+{\bullet}Py)$ complexes are both substantially smaller than the estimated binding energy of the covalent radical $(Bz{\bullet}Py)^{+\bullet}$ adduct.

3. Mobilities of the Observed Dimers. The reduced mobilities in helium of the various monomer and dimer ions are shown in Table 3. The ATDs of the $(Bz{\bullet}Py)^{\bullet+}$ adduct and the protonated

(44) Deakyne, C. A.; Meot-Ner (Mautner), M. *J. Am. Chem. Soc.* **1985**, *107*, 474.

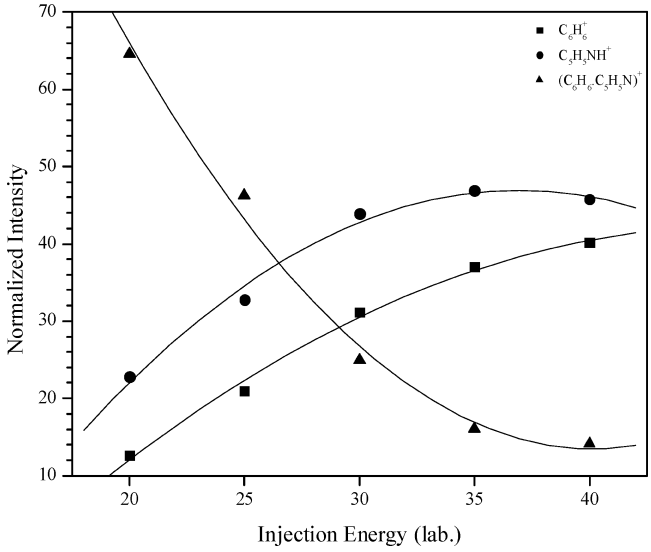

Figure 4. Effect of injection energy on the collisional dissociation of $(C_6H_6 \cdot C_5H_5N)^{\bullet+}$ adduct injected into 2.0 Torr of He (error estimate in the normalized ion intensity is ±7%).

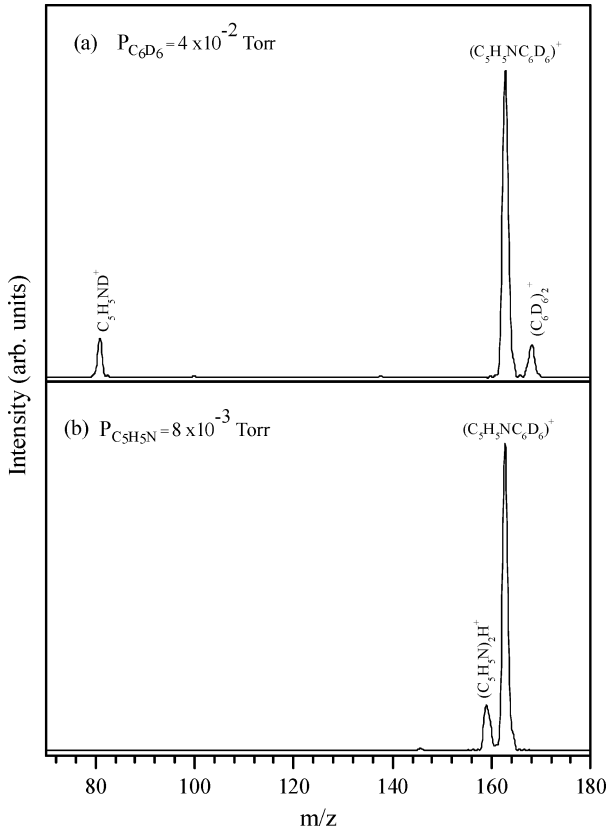

Figure 5. (a) Mass spectrum of $(C_5H_5N \cdot C_6D_6)^{\bullet+}$ injected with injection energy = 15 eV (laboratory coordinates) into C_6D_6/He at a partial pressure of $C_6D_6 = 4.0 \times 10^{-2}$ Torr in 1.5 Torr He at field of 1.85 V Torr^{-1} cm^{-1} and $T = 303$ K. (b) Mass spectrum of $(C_6D_6 \cdot C_5H_5N)^{\bullet+}$ injected at 15 eV injection energy (laboratory coordinates) into C_5H_5N/He at a partial pressure of $C_5H_5N = 8.0 \times 10^{-3}$ Torr in 2.0 Torr He at a field of 1.40 V Torr^{-1} cm^{-1} and $T = 303$ K.

pyridine dimer $PyH^+ \cdot Py$ in He at 304 K at different applied voltages across the drift cell are given in the Supporting Information (SI-3).

Mobility measurements can provide structural information on the dimers on the basis of their collision cross-sections (Ω's),

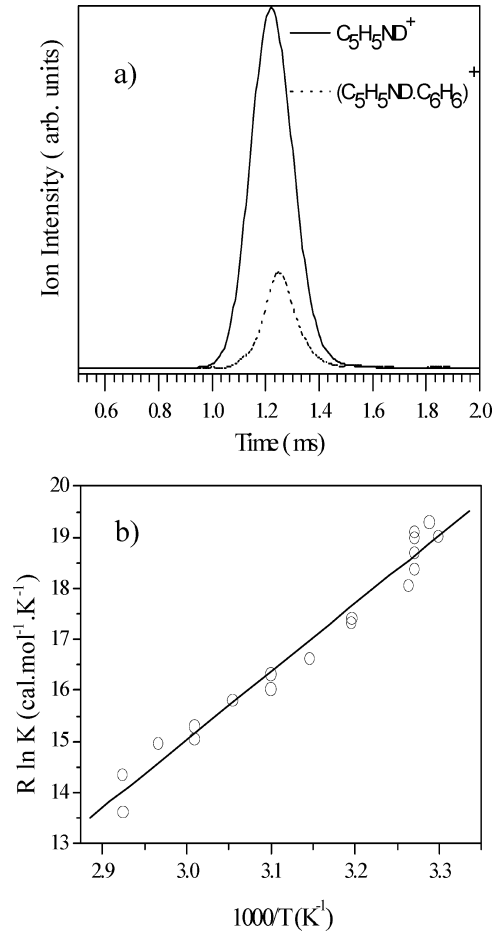

Figure 6. (a) Equal ATDs show equilibrium between $C_5H_5ND^+$ and $C_5H_5ND^+ \cdot C_6H_6$. (b) van't Hoff plot for the equilibrium $C_5H_5ND^+ + C_6H_6 = (C_5H_5ND^+ \cdot C_6H_6)$ for the formation of a dimer ion from protonated pyridine and benzene.

Table 3. Measured Reduced Mobilities (K_0, cm^2 V^{-1} s^{-1}) and the Corresponding Collision Cross-Sections (Ω, Å^2) of Monomer and Dimer Ions in the (Benzene/Pyridine)$^{\bullet+}$ and Related Systems

ion	K_0 (cm^2 V^{-1} s^{-1})	Ω (Å^2)
$C_5H_5N^{\bullet+}$	11.8 ± 0.6	46 ± 2
$C_6H_6^{\bullet+}$	11.4 ± 0.5	48 ± 2
$C_5H_5NH^+$	11.8 ± 0.6	45 ± 2
$(C_5H_5N)_2H^+$	6.9 ± 0.3	78 ± 3
$(C_6H_6)_2^{\bullet+}$	7.6 ± 0.3	71 ± 3
$(C_5H_5N \cdot C_6H_6)^{\bullet+}$	7.4 ± 0.3	73 ± 3

which depend on the geometric shapes of the ions.[19,30−32,39] Theoretical calculations of possible structural candidates of the ions are then used to compute angle averaged Ω's at different temperatures (using the trajectory method),[41] for comparison with the measured ones.

The measurements yielded reduced mobilities of 7.4 ± 0.3 and 6.9 ± 0.3 cm^2 V^{-1} s^{-1} for the $(Bz \cdot Py)^{\bullet+}$ and the $PyH^+ \cdot Py$ dimers, respectively. For comparison, the reduced mobility of the benzene dimer cation $(Bz \cdot Bz)^{\bullet+}$ that has a parallel sandwich structure is 7.6 ± 0.3 cm^2 V^{-1} s^{-1}.[19] The sandwich structure of the benzene dimer cation has been suggested on the basis of both mobility measurements and ab initio calculations.[19] The similarity between the reduced mobility of $(Bz \cdot Bz)^{\bullet+}$ and the $(Bz \cdot Py)^{\bullet+}$ dimers may suggest that both dimers have more compact structures than the $PyH^+ \cdot Py$ dimer, which could have an extended anisotropic shape. The measured mobilities can be

Table 4. Calculated Ab Initio Bond Dissociation Energies (Corrected for BSSE) and Mobilities of Isomeric Dimers in the (Benzene−Pyridine)$^{\bullet+}$ System[a]

isomer type	BDE[a,b]	BDE[a,b] with BSSE	BDE[a,c]	BDE[a,c] with BSSE	K_0[d]	Ω (Å^2)
Hydrogen-Bonded						
A	13.8	12.8			7.59	70.79
B	27.0	25.8			7.37	72.92
Covalent C−N Bonded						
C	34.1	31.3			7.51	71.55
D	38.1	31.2			7.56	71.12
E	40.1	38.1			7.54	71.25
Distonic Hydrogen Bonded						
F		20.1	10.9	10.3	6.83	78.71
G		18.8	9.9	9.0	7.18	74.84
H		18.6	9.5	8.7	7.19	74.78
I		26.4	17.3	16.6	7.06	76.07

[a] Bond dissociation energies (BDE) in kcal/mol. [b] Calculated bond dissociation energies, without and with BSSE corrections, to the $C_6H_6^{+\bullet}$ + C_5H_5N reactants. [c] Bond dissociation energies, without and with BSSE corrections, to the PyH^+ + $C_6H_5^\bullet$ monomers. [d] Mobilities for geometries optimized at UB3LYP/6-311G(d,p) level of theory; see Figures 7−9. The mobilities (cm^2 V^{-1} s^{-1}) were calculated with the trajectory method using the MOBCAL program.[41] Compare with the measured mobility of 7.4 ± 0.3 cm^2 V^{-1} s^{-1} of the $(C_6H_6{\cdot}C_5H_5N)^{\bullet+}$ adduct (Table 3).

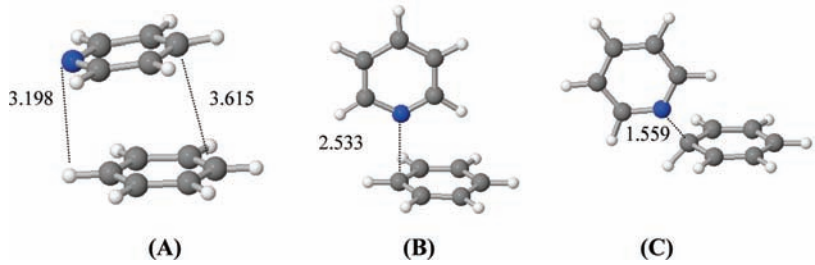

Figure 7. Optimized structures of the $(C_6H_6^{\bullet+}{\cdot}C_5H_5N)$ adduct. Mulliken charges on Bz moieties are: (A) 0.57, (B) 0.54, and (C) 0.37 (total charge on Bz + Py = 1.00). (See Supporting Information for relative energies (SI-4) and charges and bond lengths (SI-6).)

compared to the calculated mobilities based on the ab initio structures given in Table 4. These structures are discussed below.

4. Theoretical Calculations. The ab initio calculations examined several $(C_6H_6{\cdot}C_5H_5N)^{\bullet+}$ adducts, optimized at the UB3LYP/6-311G(d,p) level. The accuracy of the calculations can be assessed by comparing the energies of the charge transfer reaction (1) and proton transfer reaction (2) in Table 2 with experimental literature values. For reaction 1, the calculated value is −1.1 kcal/mol, as compared to the experimental ΔH^o of +0.4 kcal/mol. For reaction 2, the calculated value is −9.8 versus the experimental ΔH^o of −8.2 kcal/mol. In both cases, the agreement is within the uncertainties of the experimental data, and should be satisfactory considering that large, open shell-species are involved.

4.a. Structure of the Benzene−Pyridine $(C_6H_6{\cdot}C_5H_5N)^{\bullet+}$ Dimer Cation. Figure 7 shows the complexes that were optimized assuming interaction of $C_6H_6^{\bullet+}$ with pyridine, Figure 8 shows the covalently bonded isomers, and Figure 9 shows optimized structures for the distonic dimers in which $C_5H_5NH^+$ bonds to the $C_6H_5^\bullet$ radical.

Table 4 shows the calculated dissociation energies of all isomers into $Bz^{\bullet+}$ + Py. The lowest energy isomers are the covalently bonded isomers E and D. Isomer E contains a covalent C−N bond, with a proton transferred from $Bz^{\bullet+}$ to the para carbon of Py. The energy of this carbon-protonated pyridine isomer in its relaxed monomer geometry was calculated to be higher by 65.5 kcal/mol than the conventional N-protonated pyridine ion.

The measured collision cross-section of the $(C_5H_5N{\cdot}C_6H_6)^{\bullet+}$ ion (73 ± 3 Å^2) agrees well with the calculated cross-sections for all of the $(Bz{\cdot}Py)^{\bullet+}$ isomers including the lowest-energy isomer E, but is somewhat different from the calculated cross-sections of the distonic isomers, especially isomer F.

The calculated collision cross-sections of the covalent $(Bz{\cdot}Py)^{\bullet+}$ adducts D and E (Table 4) are smaller than the measured value for $PyH^+{\cdot}Py$ (Table 3), although all three have a central bond connecting two rings in a propeller-like twisted geometry (see Supporting Information). The smaller collision cross-sections of the covalent isomers may be due to the shorter central C−N covalent bond that keeps the rings closer as compared to the hydrogen-bonded $PyH^+{\cdot}Py$ dimer.

4.b. Energies of the (Benzene·Pyridine)$^{\bullet+}$ Dimer Cation Isomers. The binding energy of $(Bz{\cdot}Py)^{\bullet+}$ of >33 kcal/mol is much larger than the 17.6 kcal/mol binding energy of $Bz_2^{\bullet+}$, and no energy minima were found for $(Bz{\cdot}Py)^{\bullet+}$ with a sandwich conformation similar to the $Bz_2^{\bullet+}$ dimer. However, we observe a large fractional charge of about −0.3 on the Py N atom in all of the complexes, where this charge can interact with positive charge centers on the Bz component. Interestingly, this applies even in the covalent dimers C, D, and E, suggesting that electrostatic interactions are significant in all of these dimers. (See Supporting Information for charges and bond lengths, SI-7.)

The parallel dimer A has a local minimum of 12.8 kcal/mol in a slipped conformation with a distance of 3.198 Å between the negative N atom (−0.248) and a Bz hydrogen (+0.152). The perpendicular isomer B has significantly higher bond dissociation energy (BDE = 25.8 kcal/mol) than A. Apparently because of the negative charge on the Py nitrogen (−0.291, SI-6), no minima were found for a perpendicular geometry of the Py nitrogen atom binding to the Bz aromatic center where all carbons are negative. A binding energy of 25.8 kcal/mol was

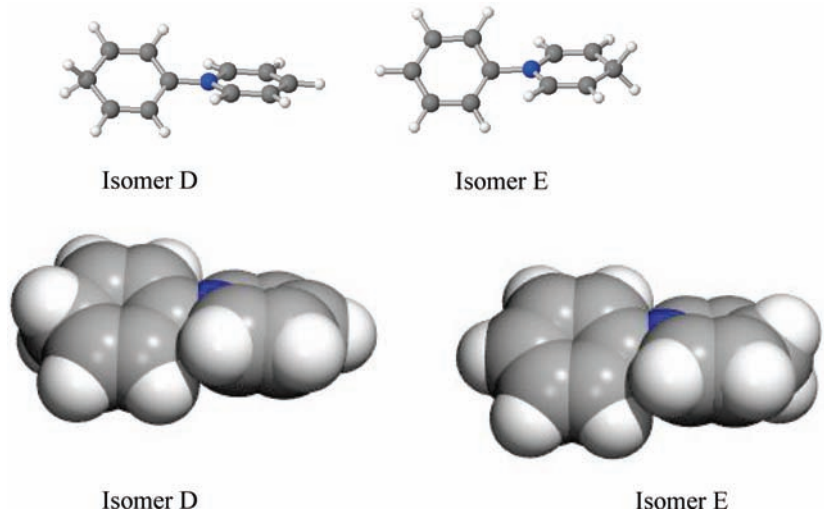

Figure 8. Structures of the covalent $(C_6H_6{-}NC_5H_5)^{\bullet+}$ and $(C_6H_5{-}NC_5H_6)^{\bullet+}$ benzene/pyridine adducts. (See Supporting Information for charges and bond lengths, SI-7.)

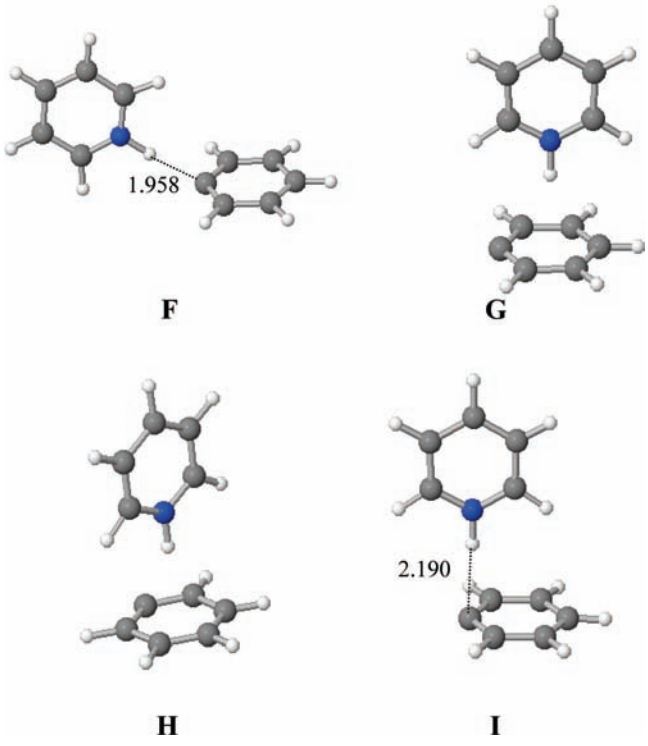

Figure 9. Optimized geometries of the $(C_5H_5NH^+{\cdot}C_6H_5^{\bullet})$ distonic dimers. Mulliken charges on $C_5H_5NH^+$ are: (F) 0.92, (G) 0.94, (H) 0.98, and (I) 0.93. (See Supporting Information for charges and bond lengths, SI-8.)

calculated, however, for the perpendicular structure B with a noncovalent C−N bond of 2.533 Å in which the negative N atom of Py interacts with one or two H atoms (+0.146, SI-6) of Bz adjacent to the C atom nearest to N (Figure 7). The structures of these noncovalent $(Bz{\cdot}Py)^{+\bullet}$ adducts suggest again that electrostatic interactions are dominant.

In isomer C (BDE = 31.3 kcal/mol), the C−N bond is covalent with a bond length of 1.593 Å. In this isomer, the N atom has a large negative charge (−0.334, SI-6), and it is bonded to a C atom of Bz that also has a small negative charge (−0.065, SI-6). However, the negative N atom may interact with the positively charged H atoms (+0.134, SI-6) on the ortho carbons of Bz.

Isomers D (BDE = 31.2 kcal/mol) and E (BDE = 38.1 kcal/mol) have covalent bonds of ∼1.42 Å between the C atom of Bz and the N atom of Py. Here, also the negative charge on the N atom (−0.395, SI-7) may interact with the positive charge on the C atom (+0.126, SI-7) of Bz to which it is bonded, and with the ortho Bz hydrogens (+0.141, SI-7), which are slightly more positive than in isomer C (+0.134, SI-7). These more favorable electrostatic interactions may be the reason for the large stability of isomers D and E. Isomer E is more stable than isomer D, and its dissociation energy of 38.1 kcal/mol is consistent with the observed bonding energy of $(Bz{\cdot}Py)^{\bullet+}$ of >33 kcal/mol that was derived above from reactivity considerations. Nevertheless, the bonding energies of C and D are small for covalent bonds. The destabilizing factors may be the distorted geometries of the protonated rings in these complexes and repulsion between the ortho hydrogens of Bz and Py that lead to propeller-like twisted geometries between the planes of the two rings (Figure 8).

4.c. Distonic Pyridine$H^+{\cdot}$Phenyl Radical Dimers. As discussed above, exothermic proton transfer may occur in the complex, which could then form the distonic $(C_5H_5NH^+{\cdot}C_6H_5^{\bullet})$ adducts (Figure 9). Here, most of the charge is on the protonated PyH^+ component that in isomers F, G, H, and I bears charges of 0.92, 0.94, 0.98, and 0.93, respectively (SI-8). While the N atom still has a negative charge of about 0.3, the N−H proton has a positive charge of about 0.3 in all of the isomers (SI-8). The proton points to a negative charge center in the $C_6H_5^{\bullet}$ ligand, leading to electrostatic interactions that determine the structures and energies of these complexes.

In dimer F and in the most stable distonic dimer I, the NH^+ proton points to the radical carbon atom of $C_6H_5^{\bullet}$ that has a lone electron pair and negative charge. These interactions are similar to $NH^+{\cdot}C$ hydrogen bonds with carbon lone pairs of isocyanide ligands.[33,44] Dimer F is only weakly bonded by 10.3 kcal/mol with respect to dissociation to the $C_5H_5NH^+ + C_6H_5^{\bullet}$ components, while the perpendicular complex I has a larger dissociation energy of 16.6 kcal/mol. In dimers G and H, the NH^+ proton points to the center of the π ring of the $C_6H_5^{\bullet}$ radical that is also in the center of carbon atoms with negative charges. This is similar to ionic hydrogen bonds in the $NH^+{\cdots}\pi$ systems consisting of protonated nitrogen and neutral aromatic ligands.[33,44]

The calculated structure shown in Figure 9 does not have hydrogen bonds, but isomer F contains a 1.958 Å bond to the C atom of the $C_6H_5^{\bullet}$ radical. This complex is only weakly bonded by 10.3 kcal/mol with respect to dissociation to the $C_5H_5NH^+ + C_6H_5^{\bullet}$ components, while the perpendicular complex I has a larger dissociation energy of 16.6 kcal/mol.

The perpendicular $NH^+\cdots\pi$ dimers G and H, where the PyH^+ proton points to the center of the $C_6H_5^{\bullet}$ ring, are more weakly bonded, with dissociation energies of 9.0 and 8.8 kcal/mol, respectively. The general finding is that hydrogen bonds to the radical carbon atom of $C_6H_5^{\bullet}$ are stronger than bonds to the more delocalized π system of the phenyl radical.

4.d. Closed-Shell Complexes of PyridineH$^+$ with Benzene and Pyridine. In the distonic complexes F−I, the closed-shell PyH^+ ion is an NH^+ hydrogen donor, which can form a $NH^+\cdot\pi$ hydrogen bond or an $NH^+\cdot$:C (carbon lone pair) bond with the phenyl radical. For comparison, we calculated the structures of the closed-shell $PyH^+\cdot$Bz complex that can also form $NH^+\cdots\pi$ bonds and the $PyH^+\cdot$Py complexes that can form $NH^+\cdots$:N (nitrogen lone pair) bonds. These complexes, along with $(Bz\cdot Py)^{\bullet+}$ above, complete the survey of stable cationic complexes in the benzene/pyridine system. The other complexes are the benzene dimer cation $(Bz\cdot Bz)^{\bullet+}$ that was studied previously,[15,18] and the pyridine dimer cation $(Py\cdot Py)^{\bullet+}$ that can disproportionate with proton transfer to form protonated pyridine PyH^+ and $C_5H_4N^{\bullet}$.

An $NH^+\cdot\pi$ hydrogen bond can form in ($PyH^+\cdot$Bz). Figure 10 shows a hydrogen bond to the negatively charged C atoms of the benzene ring in this closed-shell dimer. A T-shaped isomer with NH^+ pointing to the center of benzene ring, with an identical energy (0.01 kcal/mol less stable), was also obtained by our calculations. The observed dimers probably contain equilibrium populations of several $NH^+\cdot\pi$ bonded isomers.

A similar L-shaped structure with about 70° angle tilt between the pyridine and phenyl rings was obtained recently by coupled cluster CCSD(T) calculations of Tsuzuki et al.[35] The similarity of the low energy structures of the ($PyH^+\cdot$Bz) complex obtained by our ab initio calculations at the UB3LYP/6-311G(d,p) level and the high level CCSD(T) calculations provide some justification for the level of theory used in our calculations.

Our measured binding energy of 13.4 kcal mol^{-1} for the $PyH^+\cdot$Bz (i.e., $C_5H_5NH^+\cdot C_6H_6$) complex (Table 1) is close to the binding energy of 14.77 kcal/mol calculated by Tsuzuki et al.[35] For comparison, the measured binding energies of other ammonium cations to benzene are: NH_4^+, 19.3; $CH_3NH_3^+$, 18.8; and $(CH_3)_3NH^+$, 15.9 kcal/mol. As usual, the binding energies to the BH^+ ions decrease with increasing proton affinity of the conjugate bases B.[33] The $PyH^+\cdot$benzene complex fits this trend, as its binding energy is comparable to that of $(CH_3)_3NH^+\cdot$benzene, noting that $(CH_3)_3N$ and pyridine have comparable proton affinities.

The binding energy of the $PyH^+\cdot C_6H_6$ closed-shell dimer is larger than that of the calculated distonic $PyH^+\cdot C_6H_5^{\bullet}$ dimers G and H that also involve $NH^+\cdot\pi$ interactions, but smaller than the binding energy of 16.6 kcal mol^{-1} of dimer I with an $NH^+\cdot$C interaction with the radical carbon. This suggests again that hydrogen bonding to the radical site has an additional stabilizing effect.

Finally, we consider the closed-shell proton-bound $PyH^+\cdot$Py dimer. The lowest energy structure calculated at the UB3LYP/6-311G(d,p) level is shown in Figure 11.

As shown in Figure 11, a T-shaped H-bonding structure is found with a binding energy of 23.8 kcal/mol (corrected for BSSE) in excellent agreement with the experimental value of 25.2 kcal/mol (Table 1).[20] Furthermore, the calculated structure results in a cross-section of 80.5 Å^2, also in excellent agreement with the measured cross-section of 78 ± 3 Å^2 based on the mobility measurements (Table 3). It should be noted that the T-shaped structure of the $PyH^+\cdot$Py dimer has the largest

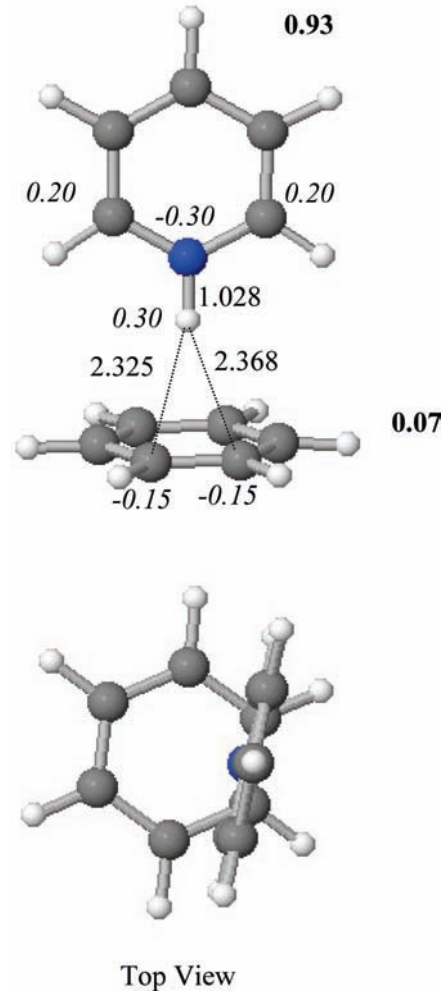

Figure 10. Geometry of the lowest energy pyridinium−benzene complex ($C_5H_5NH^+\cdot C_6H_6$) from our calculations.

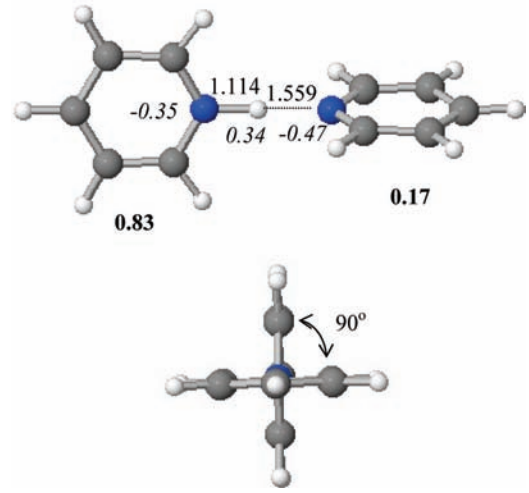

Figure 11. Optimized structure of the protonated pyridine ($C_5H_5NH^+\cdot C_5H_5N$) dimer at the UB3LYP/6-311G(d,p) level.

collision-cross-section (78 ± 3 Å^2) in comparison with the benzene dimer cation $(C_6H_6)_2^{\bullet+}$ (71 ± 3 Å^2) and the $(C_5H_5N\cdot C_6H_6)^{\bullet+}$ dimer (73 ± 3 Å^2).

Both the closed-shell ($C_5H_5NH^+\cdot C_5H_5N$) and the distonic ($PyH^+\cdot C_6H_5^{\bullet}$) dimers may form hydrogen bonds of NH^+ to N or C lone pair, respectively. However, in ($PyH^+\cdot C_6H_5^{\bullet}$), the perpendicular structure I was the most stable with a calculated bond energy of 16.6 kcal/mol (Figure 9), while the ($C_5H_5NH^+\cdot C_5H_5N$) dimer contains a linear $NH^+\cdot N$ hydrogen bond (Figure 11) with a calculated bond energy of 23.8 kcal/mol. This is consistent with the general trend that ionic hydrogen bonds of N and O donors and acceptors are stronger than carbon-based hydrogen bonds.[33,44]

4.e. Summary of Evidence about the Structure of the $(Bz\cdot Py)^{\bullet+}$ Cation. In this work, we presented experimental and computational evidence on the first observation of the $(Bz\cdot Py)^{\bullet+}$ covalent adduct. Here, we summarize the experimental and theoretical information obtained to identify the most likely structure of the observed adduct.

(1) Complexes A and B could exchange with Bz to give the $(Bz)_2^{\bullet+}$ ion, and this would be exothermic for (A). Because this reaction is not observed, isomer A can be ruled out.

(2) Complexes F−I could exchange with Py to give $PyH^+\cdot Py$. Considering the dissociation energies of these complexes to $PyH^+ + C_6H_5^{\bullet}$ in Table 4 and the binding energy of PyH^+Py (25.2 kcal/mol, Table 1), this would be exothermic for all of the distonic isomers. The absence of these exchange reactions rules out the distonic isomers. The measured cross-section of the $(Bz\cdot Py)^{\bullet+}$ adduct also does not agree well with those calculated for the distonic isomers.

(3) Threshold collisional dissociation yields mostly $PyH^+ + C_6H_5^{\bullet}$. This suggests that in the observed adduct a proton is transferred to Py. This is the case only for isomer E and the distonic isomers F−I, but the latter are ruled out as shown in (2) above. Therefore, the experimental evidence prefers isomer E.

(4) Moreover, isomer E has the lowest energy. The reactivity arguments above suggested that the binding energy of the complex is >33 kcal/mol, and only isomer E has this binding energy.

Therefore, the combination of the experimental and computational evidence suggests that E is in fact the observed isomer.

IV. Conclusions

The adduct $(Bz\cdot Py)^{\bullet+}$ is the main (>90%) product of thermal reactions in the ionized Bz/Py system under our conditions. Reactions at higher energies also produce the proton transfer products $PyH^+ + C_6H_5^{\bullet}$ and charge transfer products. Both the experimental and the theoretical results suggest that the adduct $(Bz\cdot Py)^{\bullet+}$ is covalently bonded with a binding energy of >33 kcal mol^{-1} based on ligand-exchange tests, consistent with the calculated binding energy of 38.1 kcal mol^{-1} of the covalent isomer E. Evidence from collisional dissociation, reactivity, and mobility is all consistent with the covalently C−N bonded $(C_6H_5-NC_5H_6)^{\bullet+}$ dimer as the observed adduct.

The covalent bond may be weakened by the distortion of the C-protonated pyridine ring and by steric and electrostatic intracomplex interactions. Comparison with the benzene dimer cation shows that, while $Bz_2^{\bullet+}$ has a parallel sandwich geometry stabilized by charge transfer resonance, the partial negative charge on the pyridine N atom leads in $(Bz\cdot Py)^{\bullet+}$ to geometries and charge distributions that suggest primarily electrostatic stabilizing interactions.

Further, the ab initio calculations identified several possible distonic species. Distonic ions are usually formed by intramolecular H atom transfer leaving a separate radical and protonated site in one ion. In comparison, the ($C_5H_5NH^+\cdot C_6H_5^{\bullet}$) distonic complexes are formed by intermolecular proton or H atom transfer between two components of a dimer. In the resulting distonic dimers, the charge resides on one component and the radical site on another component of the complex. Isomers of the distonic dimers are stabilized by $NH^+\cdot C$ and $NH^+\cdot\pi$ type ionic hydrogen bonds. The computations show that hydrogen bonding to the radical carbon provides extra stability over hydrogen bonding to the π-system of the phenyl radical.

The distonic dimers can be intermediates in the high-energy dissociation of the complex. Collisional dissociation can produce $C_5H_5N^{\bullet+} + C_6H_6$, or $C_6H_6^{\bullet+} + C_5H_5N$, or $C_5H_5NH^+ + C_6H_5^{\bullet}$, suggesting that the classical and distonic forms can interconvert at high energies.

The deep energy well of the covalent adduct results in a long enough lifetime so that all of the complexes are stabilized at about 1 Torr. The large number of degrees of freedom in these adducts may allow them to be stabilized also radiatively, in competition with charge or proton transfer, even at low pressures in space environments. The chemistry at higher pressures will be of interest with respect to solar nebula chemistry, where gases are subjected to ionizing radiation under relatively high gas densities, which can allow the formation of adducts and complex polycyclic organic molecules. Such processes can lead to the cross-linked polymers found in meteorites.

The formation of (benzene/pyridine)$^{\bullet+}$ adduct may represent a general class of addition reactions. For example, we also observed the irreversible additions of pyridine$^{\bullet+}$ to ethylene, propene, and acetylene (to be reported elsewhere), under conditions similar to those reported in this work. Covalent addition of ionized nitrogen heterocyles to unsaturated hydrocarbons may therefore be a general class of reactions that can form complex heterocyclic species in ionizing environments and in space.

Acknowledgment. We gratefully acknowledge NASA for the support of this research through grants NNX08AI46G and NNX07AU16G.

Supporting Information Available: Arrival time distributions and mass spectra data (SI-1−SI-3), relative energies, Mulliken charge distributions and bond lengths of calculated isomers (SI-4−SI-8), and complete ref 42 (SI-9). This material is available free of charge via the Internet at http://pubs.acs.org.

JA901130D